ARCHIVES
of
FOUNDRY ENGINEERING

ISSN (2299-2944)
Volume 2026
Issue 3/2026

110 – 119

13/3

10.24425/afe.2026.158024

Published quarterly as the organ of the Foundry Commission of the Polish Academy of Sciences

Thermodynamic Analysis of MnS Inclusion Precipitation in Non-Quenched and Tempered 46MnVS5 Steel

Huakang Sun [a], Shuhuan Wang [a], Pengju Li [b], Yuekai Xue [a, *]
[a] North China University of Science and Technology, China
[b] HBIS Group Shisteel Company, Shijiazhuang, China
* Corresponding author. E-mail address: 13292532767@163.com

Received 03.07.2026; accepted in revised form 27.08.2026; available online 23.09.2026

Abstract

Based on the theories of thermodynamic equilibrium and non-equilibrium solidification, this paper systematically investigated the precipitation behavior of MnS inclusions during the solidification of non-quenched and tempered 46MnVS5 steel. By calculating the standard Gibbs free energy change, equilibrium constant, activity coefficient, and liquidus and solidus temperatures for the MnS formation reaction, and combining these with the Scheil-Gulliver model and FactSage 8.1 software, this study analyzed the changes in the concentration product, the conditions for the onset of precipitation, the patterns of element segregation, and the influence of alloying element content during the solidification process. The results indicate that MnS precipitation is jointly controlled by temperature reduction and the enrichment of Mn and S elements, with substantial precipitation occurring primarily during the late stage of solidification (solid fraction > 0.95); the Scheil model predicts a precipitation onset temperature of 1290 °C and a final MnS mass fraction (relative to the total system mass) of approximately 0.09%; the contents of C, Mn, and S significantly influence MnS precipitation behavior, while those of Al, Si, and P have a negligible effect. These findings provide a theoretical basis for controlling the morphology of MnS inclusions in non-quenched and tempered steels.

Keywords: 46MnVS5 steel, MnS inclusions, Thermodynamic calculations, Segregation behavior

1. Introduction

Non-quenched-and-tempered steels are widely used in the manufacture of structural components for automobiles, construction machinery, and other applications [1-4] because they eliminate the quenching-and-tempering process, are energy-efficient and environmentally friendly, and offer excellent overall mechanical properties. As a typical medium-carbon non-quenched-and-tempered steel, the key to optimizing the properties of 46MnVS5 lies in controlling inclusions, particularly MnS inclusions. MnS inclusions not only affect the steel's machinability but also significantly influence its toughness, fatigue life, and anisotropy [5-10].

The precipitation behavior of MnS inclusions is essentially governed by a combination of the temperature field, solute redistribution, and local concentration fluctuations during solidification [11-14]. In recent years, thermodynamic calculation methods have become an important tool for elucidating the mechanisms of inclusion precipitation; however, existing studies have largely focused on equilibrium analyses, and systematic research on the coupling mechanism between MnS precipitation kinetics and element segregation under non-equilibrium solidification conditions remains limited [15-18].

© The Author(s) 2026. Open Access. This article is licensed under a Creative Commons Attribution 4.0 International License (http://creativecommons.org/licenses/by/4.0/), which permits use, sharing, adaptation, distribution and reproduction in any medium or format, as long as you give appropriate credit to the original author(s) and the source, provide a link to the Creative Commons licence, and indicate if changes were made.

Although extensive studies have been conducted on MnS precipitation in various medium-carbon non-quenched and tempered steels such as 49MnVS3 [15, 19], 45MnVS [7], and U75V [18], these investigations primarily focus on the final precipitation characteristics without systematically elucidating the dynamic coupling between solute segregation and precipitation kinetics under non-equilibrium conditions. Furthermore, a comprehensive comparative analysis of how different alloying elements differentially regulate precipitation behavior in the specific 46MnVS5 system is still lacking. To address this gap, this study systematically investigates the precipitation patterns of MnS inclusions, the characteristics of elemental segregation, and the influence mechanisms of key alloying elements during the solidification of 46MnVS5 steel using FactSage 8.1 software in conjunction with the Scheil-Gulliver model and equilibrium phase diagrams. The findings aim to provide theoretical support for the precise control of MnS inclusions in industrial production.

2. Thermodynamic Calculation Methods and Parameters

Thermodynamic calculations can be used to determine energy changes, phase transformations, and precipitation in a system at equilibrium. Sulfur (S) is a prone-to-segregation element in steel; the Gibbs free energy generated by the MnS reaction and the calculated solubility of MnS can serve as criteria for determining whether MnS precipitation can occur in molten steel. When the concentration product of Mn and S enriched in the liquid phase between dendrites exceeds the thermodynamic equilibrium solubility of MnS in the molten steel, MnS will precipitate in the form of MnS inclusions [19-21]. Table 1 shows the chemical composition of 46MnVS5 produced by a certain steel mill; this steel grade was selected for thermodynamic calculations of MnS inclusion precipitation.

Table 1.
Element composition of 46MnVS5 steel (wt%)

C	Si	Mn	P	S	V	Al	N
0.45	0.54	1.3	0.02	0.03	0.15	0.008	0.012

To better determine the timing of MnS precipitation in steel, calculations can be performed using the thermodynamic reaction equation for MnS formation and precipitation and the corresponding standard Gibbs free energy change equation (1):

$$[Mn]+[S]=MnS(s)$$
$$\Delta G^{\theta} = -167,360 + 89.21T \quad (J/mol) \tag{1}$$

Where the standard Gibbs free energy change for the MnS formation reaction is a function of temperature T (in K). The equilibrium constant K for this reaction is:

$$\ln K = \frac{-\Delta G^{\theta}}{RT} \tag{2}$$

Where R is the ideal gas constant (8.314 J/mol·K).

The actual change in Gibbs free energy during the precipitation of MnS inclusions in the solidification of molten steel is given by:

$$\Delta G = \Delta G^{\theta} + RT \ln \frac{a_{[MnS]}}{a_{[Mn]} \cdot a_{[S]}} \tag{3}$$

Where:
$a_{[MnS]}$、$a_{[Mn]}$ and $a_{[S]}$ are the activities of pure MnS and of elements Mn and S in molten steel, respectively. Since pure solid MnS is in its standard state, $a_{[MnS]} = 1$.

The activities of Mn and S can be expressed as $a_{[MnS]} = f_{Mn} \cdot \omega_{Mn}$ and $a_{[S]} = f_S \cdot \omega_S$, where ω_{Mn} and ω_S are the mass fractions of Mn and S in molten steel, and f_{Mn} and f_S are the corresponding activity coefficients.

Using a 1% solution as the reference state, the activity coefficients of the constituents in molten steel were obtained as:

$$\lg f_i = \sum e_i^j [\%j] \tag{4}$$

Where:
e_j^i—the interaction coefficient between element j and element i in the molten steel;
[%j]—the mass fraction of element j in the molten steel.

The interaction coefficients of common elements in steel are shown in Table 2.

Table 2.
Element interaction coefficients (%, 1600 °C)

Constituent	C	Si	Mn	P	S	Al	N	O
Mn	-0.07	0	0	-0.0035	-0.048	0	-0.150	-0.083
S	0.11	0.063	-0.026	0.029	-0.028	0.035	0.01	-0.27

The melting point of pure iron is TM = 1811 K(1538 ℃). The liquidus and solidus temperatures of molten steel can be obtained from Equations (5) and (6), respectively，

$$T_{liq} = 1811 - \sum \Delta T_{liq,j} \cdot [\%j] \tag{5}$$

$$T_{sol} = 1811 - \sum \Delta T_{sol,j} \cdot [\%j] \cdot \tag{6}$$

Where:
T_{liq}—Effect of a 1% concentration of alloying element j on the liquidus point (K);
T_{sol}—Effect of a 1% concentration of alloying element j on the solidus point (K).

The specific values are shown in Table 3.

Table 3.
Coefficients of the effects of various elements on the temperatures of the liquidus and solidus lines

Elements	C	Si	Mn	P	S	Al
Liquidus line	65	8	5	30	25	3
Solidus line	175	20	30	280	575	7.5

Substituting the composition of the experimental steel into the calculation yields The liquidus temperature is 1770 K (1497 ℃), and the solidus temperature is 1660 K (1387 ℃).

3. Results and Discussion

3.1. Precipitation Criterion Based on Concentration Product

This can generally be used to determine the range of values for variables (such as temperature and molar concentration of molten steel) under which a reaction occurs. When the reaction proceeds spontaneously in the forward direction, MnS inclusions can form. Here, we take temperature T as the variable and examine the relationship between the equilibrium concentration product and temperature T at equilibrium in the molten steel. When the reaction reaches equilibrium, $\Delta G = 0$,

$$\ln K = -\frac{\Delta G^{\theta}}{RT} \tag{7}$$

When the reaction reaches equilibrium,

$$\frac{a_{MnS}}{a_{[Mn]}a_{[S]}} = K \tag{8}$$

Since the activity of pure solid MnS is 1,

$$\frac{1}{f_{Mn}\omega_{Mn} \cdot f_S\omega_S} = K \tag{9}$$

$$f_{Mn}\omega_{Mn} \cdot f_S\omega_S = \frac{1}{K} \tag{10}$$

Setting Equation (7) equal to Equation (10) yields the equilibrium concentration product in the molten steel at equilibrium,

$$K_{sp} = (\omega_{Mn} \cdot \omega_S)_{eq} = \frac{1}{f_{Mn}f_S K} \tag{11}$$

As the temperature decreases, the solubility of elements in non-quenched and tempered steel decreases. In the solid-liquid two-phase region, elements continuously accumulate, leading to segregation. The actual concentration product and equilibrium concentration product of manganese and sulfur in steel are,

$$K_{sp} = \omega_{Mn} \cdot \omega_S \tag{12}$$

$$Q = \omega_{Mn(l)} \cdot \omega_{S(l)} \tag{13}$$

Where:
$\omega_{Mn(l)}$ and $\omega_{S(l)}$—Mass fractions of Mn and S in the liquid phase at the solidification front, %;
ω_{Mn} and ω_S—Mass fractions of Mn and S when the reaction reaches equilibrium , %；
T—The temperature at the solidification front, K.

According to the Scheil-Gulliver equation (assuming no diffusion in the solid phase and complete mixing in the liquid phase), the relationship between the solute concentration C_l in the liquid phase at the solidification front and the solidification fraction f_s is:

$$C_l = C_0(1 - f_s)^{k_0 - 1} \tag{14}$$

Where:
C_0 —Initial concentration of the solute,
k_0—Equilibrium partition coefficient.

The relationship between the solidification front temperature T and the solidification fraction f is given by the following equation (15),

$$T = T_{liq} - (T_{liq} - T_{sol}) \cdot f_s \quad (15)$$

By combining the above equations, we can derive a criterion for the precipitation of MnS during the solidification process:

$$K_{sp}(T) = \omega_{Mn}(T) \cdot \omega_S(T) \quad (16)$$

$$Q(T) = \omega_{Mn(l)}(T) \cdot \omega_{S(l)}(T) \quad (17)$$

When $Q(T)>K_{sp}(T)$, MnS inclusions begin to precipitate.

Figure 1 shows the variation of the actual concentration product and the standard concentration product during solidification as a function of the solidification fraction, calculated using the above formula. In the early stages of solidification (when the solidification fraction is small), the actual concentration product is lower than the standard concentration product. As solidification progresses, Mn and S in the solid phase gradually become enriched in the liquid phase [22,23]. When the solidification fraction is less than 0.95, the solubility of MnS is high, and Mn and S exist primarily in the dissolved state; when the solidification fraction exceeds 0.95, as the temperature decreases and solidification continues, the actual concentration product rises rapidly and exceeds the standard concentration product, indicating the onset of MnS inclusion precipitation. The intersection point of the two curves in the figure represents the critical point for MnS inclusion precipitation.

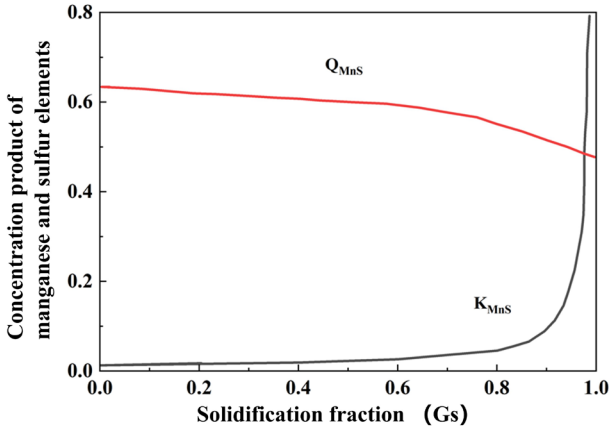

Fig. 1. Patterns of MnS precipitation during solidification

3.2. Calculations of Non-Equilibrium Solidification Based on the Scheil-Gulliver Model

During the cooling of molten steel, if the entire system reaches thermodynamic equilibrium, the diffusion of all elements is unrestricted, ultimately resulting in a fully equilibrated microstructure [24]. However, in actual production, it is very difficult to achieve this ideal state. For the solidification of molten steel, because the diffusion coefficients of solute elements in the solid phase are extremely small, the solidification process is better described by the Scheil-Gulliver model, which assumes no diffusion in the solid phase while the liquid phase remains thoroughly mixed, and assumes that local equilibrium is always achieved at the solid-liquid interface. In this section, we will use the thermodynamic calculation software FactSage 8.1 to perform computational analysis of non-equilibrium solidification behavior under extremely rapid cooling rates.

As shown in Figure 2, the calculation results indicate that when the liquid phase temperature decreases from 1600 ℃ to 1476 ℃, a large amount of material begins to precipitate, with ferrite being the first phase to precipitate from the liquid phase. When the temperature drops to 1473 ℃, the ferrite completely transforms into austenite (FCC) within a short period of time. As cooling continues, the austenite phase continuously precipitates, and the liquid phase gradually decreases. When the solid fraction reaches 0.95, the liquid phase temperature drops to 1290 °C. At this point, MnS begins to precipitate, and its content continues to increase as the temperature decreases, eventually reaching a mass fraction of approximately 0.09% relative to the total system mass, as shown in Figure 3. This value is directly obtained from the FactSage Scheil-Gulliver simulation, where the mass of precipitated MnS at each solid fraction is divided by the total system mass to yield the mass fraction. The calculation accounts for all phases present in the system and ensures mass conservation throughout the solidification process. During further cooling, carbide-rich phases begin to precipitate from the steel toward the end of solidification. Under equilibrium conditions, however, these carbide phases typically precipitate only from the solid phase. However, in the Scheil-simulated solidification process, the rapid enrichment of solute elements such as carbon (C) in the remaining liquid phase causes the carbide-rich phase to precipitate prematurely. This phenomenon indicates that the distribution of solute elements under non-equilibrium solidification conditions has a significant impact on phase transformation behavior.

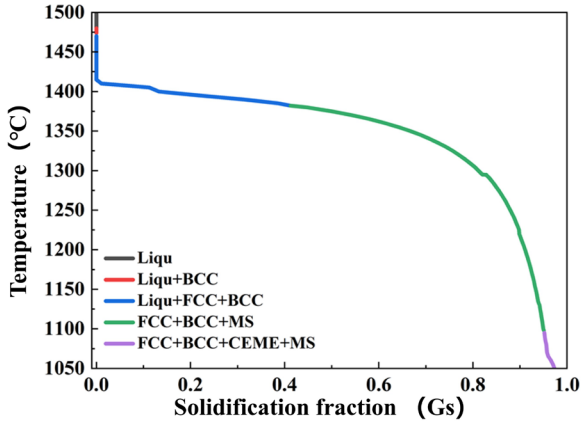

Fig. 2. Scheil calculations for the solidification process of molten steel

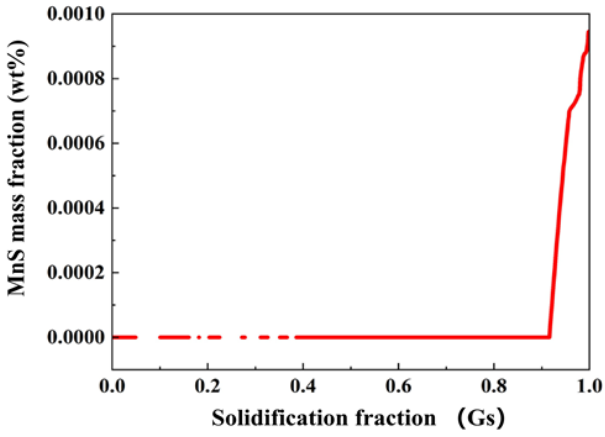

Fig. 3. Mass fraction of precipitated MnS (relative to the total system mass) as a function of solid fraction f_s, calculated using the FactSage Scheil-Gulliver model

It should be noted that Equation (15) is a simplified linear approximation between temperature and solid fraction, which does not account for the solute enrichment that depresses the actual liquidus temperature during the later stages of solidification. In contrast, the Scheil-Gulliver calculation performed with FactSage 8.1 inherently considers the coupled effects of segregation and phase equilibria, thus yielding a lower precipitation temperature (1290 °C at f_s=0.95) compared to the linear estimate (~1393 °C). The difference arises from the different treatment of solute redistribution. Therefore, Equation (15) is only suitable for rough preliminary estimates, while the FactSage Scheil result is more reliable for predicting the actual precipitation conditions under non-equilibrium solidification. The value of 1290 °C at f_s=0.95 is a direct output of the Scheil simulation and is consistent with the criterion $Q(T)>K_{sp}(T)$ shown in Figure 1.

3.3 Segregation and Distribution of Alloying Elements During Solidification

Elemental segregation primarily results from differences in the solubility of alloying elements in the liquid and solid phases at different temperatures. When the solubility of a solute element is higher in the liquid phase, it tends to accumulate in the liquid phase, resulting in positive segregation; Conversely, when the solubility of a solute element is higher in the solid phase, it accumulates in the solid phase, leading to negative segregation.

Using the Scheil model in the equilibrium module of the FactSage software, the mass fractions of alloying elements in the solid phase has been calculated during the solidification process. As shown in Figure 4, the mass fractions of Al, S, Mn, P, Si and C in the solid phase all exhibit a generally decreasing trend as the solid fraction (f_s) increases. This decreasing trend is physically consistent with their positive segregation behavior: These elements have equilibrium partition coefficients k_0<1, meaning they are preferentially rejected from the solidifying front into the residual liquid, thereby becoming progressively depleted in the solid phase [25, 26]. The slope of the curves indicates that Al is depleted from the solid phase at the fastest rate among these elements.

It is particularly noteworthy that when the solid fraction reaches approximately 0.95, the mass fraction of S in the solid phase exhibits a sharp decrease (Figure 4b). This phenomenon is a direct consequence of the massive precipitation of MnS inclusions at this stage. In the Scheil-Gulliver model, the solid composition at any instant is in local equilibrium with the surrounding liquid, i.e., $C_s=k_0 \cdot C_l$. When MnS precipitates extensively, it rapidly consumes dissolved sulfur from the residual liquid, causing the liquid-phase sulfur content C_l to drop sharply. The solid phase formed immediately afterward inherits this reduced sulfur level, thus exhibiting the corresponding sharp decline. This behavior provides strong corroborative evidence for the MnS precipitation criterion established in Section 3.1 (Figure 1), where the concentration product Q is shown to exceed K_{sp} at the same solid fraction. In contrast, the other elements (Al, Mn, P, Si, and C) do not show such a pronounced drop because they are not consumed by precipitation in significant amounts during this interval.

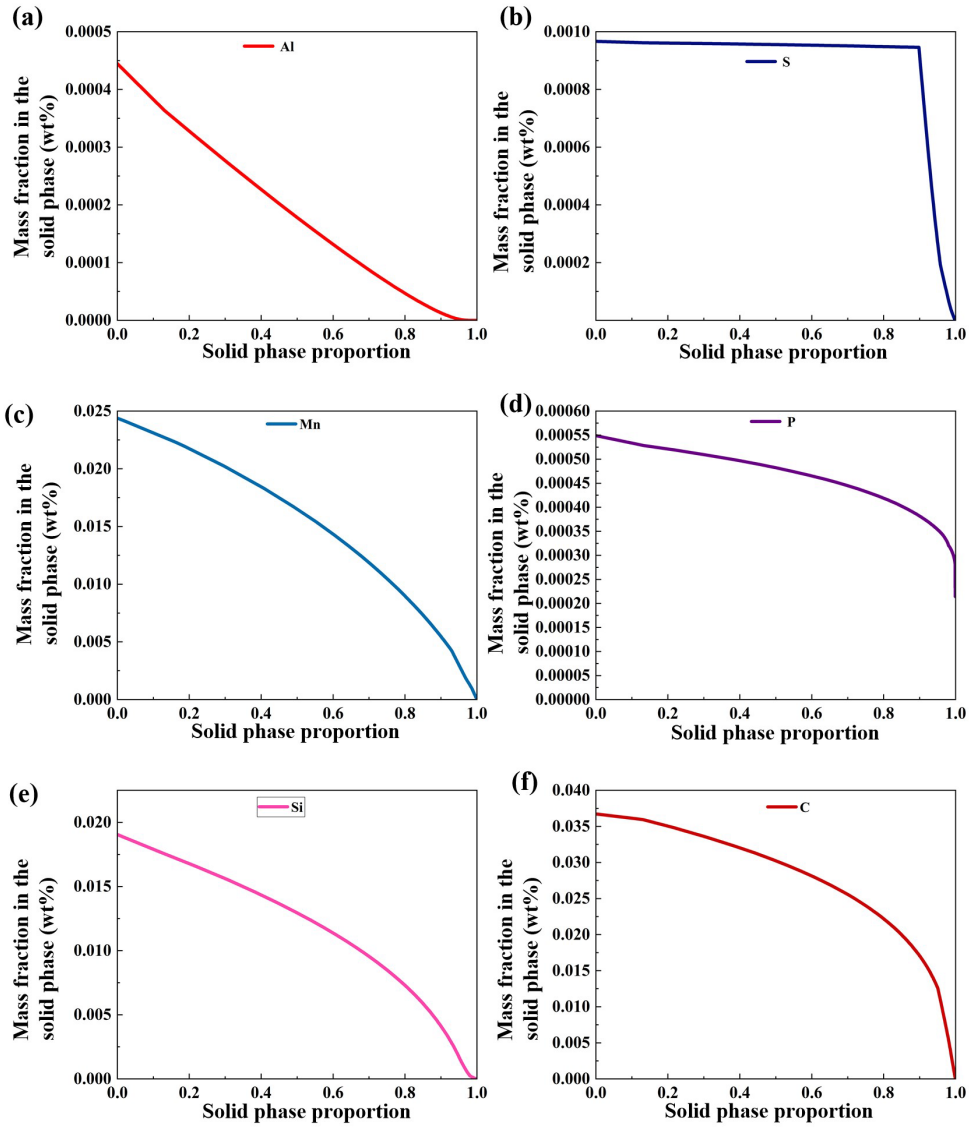

(a)—Al; (b)—S; (c)—Mn; (d)—P; (e)—Si; (f)—C.

Fig. 4. Mass fraction of solute elements in the solid phase as a function of solidification fraction f_s.

3.4. Thermodynamic Phase Diagram Analysis of MnS Precipitation in the Equilibrium Solidification Process

3.4.1 Analysis of Equilibrium Precipitation Phase Diagrams

Based on the composition of the experimental steel, the Equilib module was selected in FactSage 8.1 software, and the FSstel and FTmisc databases were used to calculate the equilibrium phase diagrams for the possible phases in the experimental steel within the temperature range of 600-1600 °C.

As shown in Figure 5, the temperature at which MnS begins to precipitate lies within the solid-liquid two-phase region. Figure 5(b) is a magnified section of the equilibrium phase diagram for the experimental steel. Initially, δ-ferrite appears at 1476 °C, which immediately transforms into austenite. MnS also precipitates in the austenite region at a temperature of 1382 °C, reaching its maximum precipitation at 1014 °C; The liquid phase ends at 1372 °C; at this temperature, MnS inclusions account for 89% of the total, indicating that MnS inclusions precipitate in large quantities during the final stage of solidification [27].

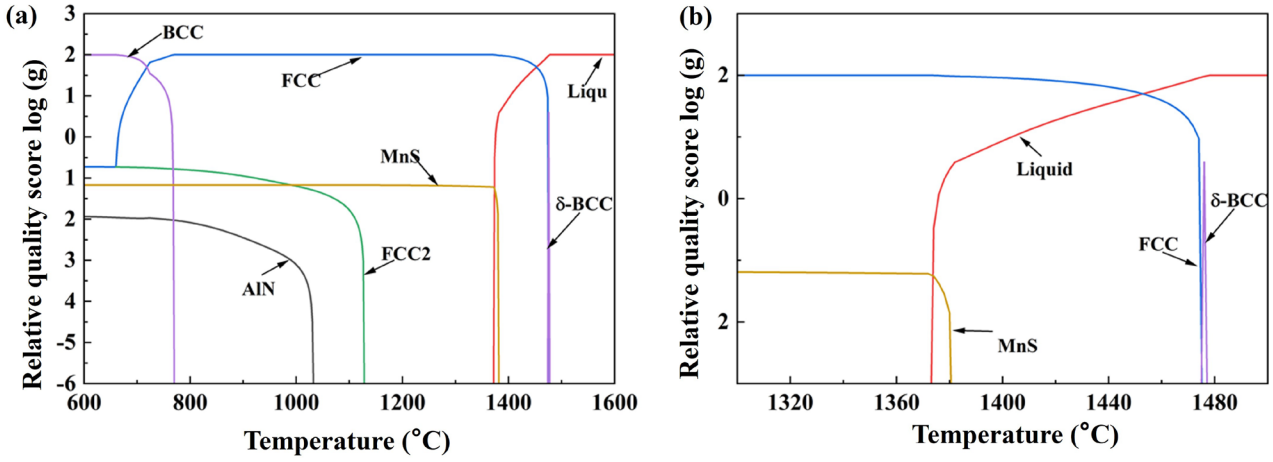

(a)—Equilibrium phase diagram; (b)—Detailed view.

Fig. 5. Experimental steel equilibrium phase diagram and MnS precipitation amount

3.4.2 Effect of Changes in Solute Element Content on MnS Precipitation

Using the thermodynamic calculation software FactSage 8.1, the effects of changes in the concentrations of base elements in the experimental steel on the precipitation temperature and amount of MnS were calculated. Using the Equilib module in the software and selecting the FSstel and FTmisc databases, the concentrations of C (0.1%-0.7%), Mn (0.05%-3%), Al (0.001%-0.1%), Si (0.03%-2.0%), P (0.001%-0.1%), and S (0.001%-0.2%) were varied. The relatively wide concentration ranges were chosen to systematically reveal the general regulatory trends of each element on MnS precipitation, covering both sub-stoichiometric and super-stoichiometric conditions relative to the nominal composition of 46MnVS5 steel. This approach allows the sensitivity and critical thresholds of each element's influence to be identified, and provides a theoretical reference for industrial composition control. The discussion of the calculation results, however, focuses primarily on the composition range relevant to the actual 46MnVS5 steel. The study calculated and analyzed the effect of changes in these base element concentrations on MnS precipitation. The calculations showed that changes in Al, Si, and P concentrations had a negligible effect on MnS precipitation, with the curves almost overlapping; therefore, Al was used as the representative element.

As shown in Figure 6, changes in the concentrations of C, Mn, and S have a significant effect on MnS precipitation and exhibit different patterns, whereas changes in the Al concentration have a relatively minor effect on the MnS precipitation process. Although there are some slight effects, they result in almost no noticeable changes in the initial precipitation temperature or the amount of MnS precipitated, as shown in Figure 6(e). As the C content increases, the MnS precipitation temperature gradually decreases, but the precipitation yield remains largely unchanged. For every 0.1% increase in C content, the MnS precipitation temperature decreases by approximately 15 °C. Conversely, an increase in Mn content leads to a rise in the MnS precipitation temperature but has a minor effect on the MnS precipitation yield. Judging from the variation curve of MnS precipitation amount at high Mn contents, high Mn content promotes rapid MnS precipitation at higher temperatures. The effect of increasing S content on MnS precipitation is similar to that of Mn: as S content increases, the precipitation temperature of MnS rises, and the precipitation amount also increases. In contrast, although an increase in Mn content also raises the MnS precipitation temperature, its effect on the precipitation yield is relatively minor. This suggests that the MnS precipitation yield may be controlled by the relative enrichment of Mn and the sulfur content.

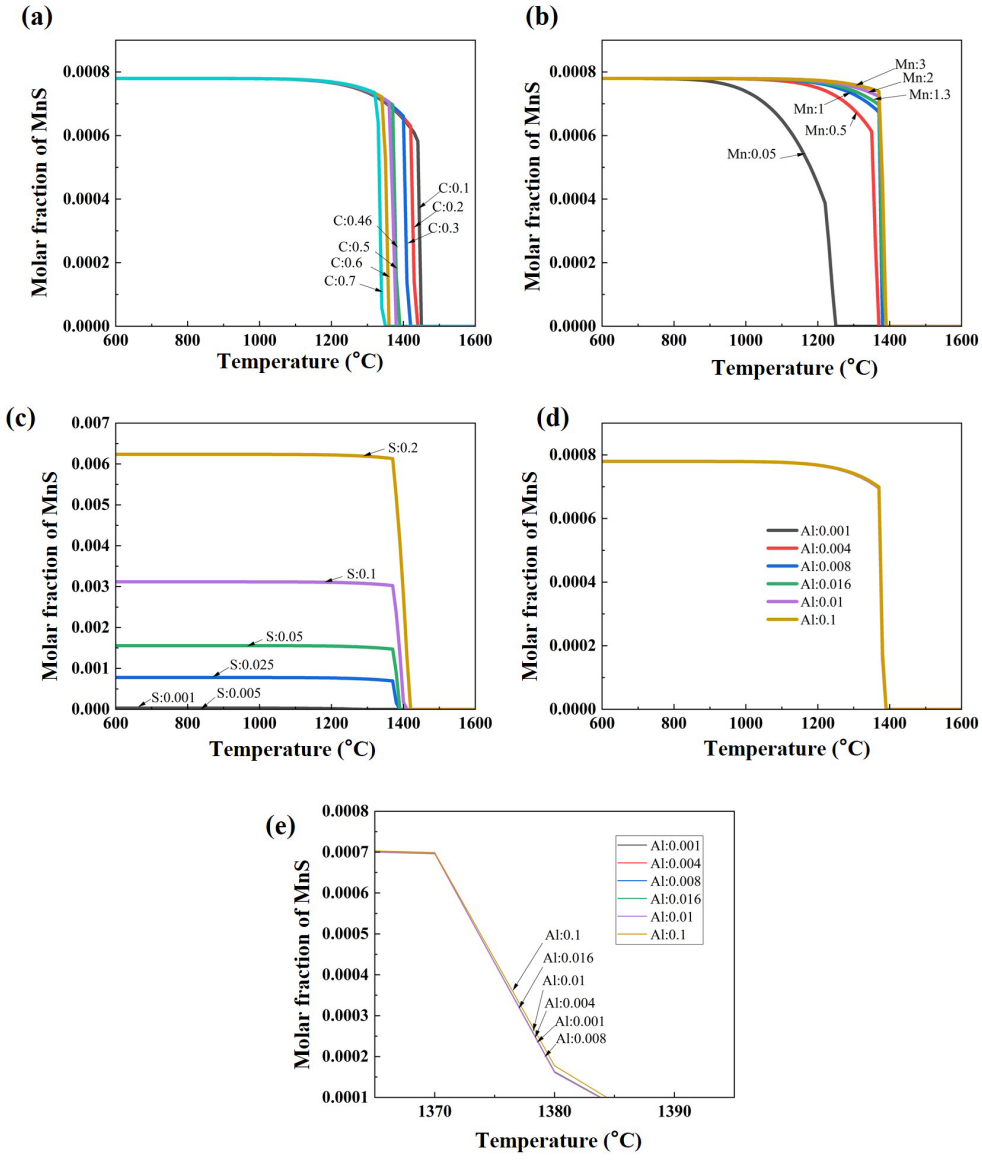

(a)—C; (b)—Mn; (c)—S; (d)—Al; (e)—close-up of Al.

Fig. 6. The effect of changes in solute element content on MnS precipitation

During solidification, due to uneven cooling rates, the element concentrations at the edges of the casting rapidly migrate toward the central liquid phase, resulting in positive segregation of the elements. Therefore, determining an appropriate cooling rate to ensure uniform cooling throughout the casting is an effective method for addressing the problem of element segregation.

3.5. Discussion

Based on the above thermodynamic calculations and analysis, the precipitation behavior of MnS inclusions during the solidification of 46MnVS5 steel can be summarized as the following key mechanisms:

1) Temperature-driven mechanism. The solubility of MnS decreases as the temperature drops; the liquidus and solidus temperatures are 1770 K and 1660 K, respectively. Toward the end of solidification (when the solid fraction exceeds 0.95), the temperature has fallen below 1290 °C, causing the solubility to drop sharply and providing the thermodynamic driving force for the massive precipitation of MnS.

2) Mechanism of solute redistribution and enrichment. Since the partition coefficient of Mn and S in the solid phase is less than 1, both elements continuously enrich in the residual liquid phase during solidification. The actual concentration product $Q=\omega_{Mn(l)}\cdot\omega_{S(l)}$, continues to rise as solidification proceeds; when it exceeds the equilibrium concentration product K_{sp}, MnS begins to precipitate. This critical condition is satisfied when the solid-phase fraction is approximately 0.95.
3) Non-equilibrium solidification effects. Actual solidification more closely resembles the Scheil-Gulliver model than a fully equilibrium model; diffusion constraints in the solid phase exacerbate solute segregation, causing the MnS precipitation temperature (1290 °C) to be lower than the value predicted by the equilibrium phase diagram (1382 °C), and resulting in a more narrow precipitation window.
4) Strategies for controlling chemical composition. The effects of C, Mn, and S content on MnS precipitation behavior each have distinct characteristics: C primarily controls the precipitation temperature window; Mn affects both the precipitation temperature and kinetics; and S influences both the temperature and the amount of precipitation. The effects of Al, Si, and P are negligible. In industrial production, appropriately reducing the S content, optimizing the Mn/S ratio, and controlling the C content range can effectively regulate the precipitation temperature and amount of MnS, thereby improving the morphology and distribution of inclusions.

4. Conclusions

a. The thermodynamic condition for MnS precipitation is that the actual concentration product exceeds the equilibrium concentration product, $\omega_{Mn(l)}\cdot\omega_{S(l)} > Ksp$. This critical condition is reached at the end of solidification (solid fraction > 0.95), at which point MnS begins to precipitate in large quantities.
b. Non-equilibrium solidification calculations based on the Scheil-Gulliver model indicate that the initial temperature for MnS precipitation is 1290 °C (solid fraction 0.95). As the temperature decreases, the amount of precipitation continues to increase, ultimately reaching a mass fraction of approximately 0.09% relative to the total system mass, as directly obtained from the FactSage simulation output. Under non-equilibrium solidification conditions, solute elements such as C become enriched in the residual liquid phase, leading to the premature precipitation of a carbon-rich carbide phase.
c. During solidification, the mass fractions of Al, S, Mn, P, Si, and C in the solid phase decrease with increasing f_s, indicating positive segregation ($k_o < 1$). Al is depleted fastest. At $f_s \approx 0.95$, the solid-phase S content drops sharply due to massive MnS precipitation, which consumes dissolved S from the residual liquid. This drop agrees with the $Q > K_{sp}$ criterion. Other elements show no such abrupt decline as they are not consumed by precipitation during this stage.
d. Analysis of the equilibrium phase diagram shows that MnS precipitates in the austenite region at a temperature of 1382 °C; by the time the liquid phase completely disappears at 1372 °C, the amount of MnS precipitated has already reached 89% of the total.

Acknoweledgments

Funding sources: 1. Yanzhao Iron and Steel Laboratory Regional Innovation Capability Enhancement Project: YZISL2024053. 2. Natural Science Foundation of Hebei Province, Project E2023209107.

References

[1] Sun, H.K., Li, Y.H., Li, P.J., Wang, S.H., Lu, B.X. & Xue, Y. K. (2026). Effect of cooling rate on the precipitation behavior of MnS inclusions in 46MnVS5 non-quenched and tempered steel. *Metalurgija*. 65(4), 321-329. https://doi.org/10.64486/m.65.4.1.
[2] Li, M.L., Wang, F.M., Tao, S.F. & Li, T.S. (2014). Solidification process and sulfide precipitation behavior in free-cutting non-quenched and tempered steel. *Transactions of Materials and Heat Treatment.* 35(4), 84-89. DOI:10.13289/j.issn.1009-6264.2014.04.016.
[3] Halfa, H. (2022). Microstructure–wear resistance relationship of nitrogen-containing high-speed tool steel, AISIM41: non-equilibrium solidification. *Metallography, Microstructure, and Analysis*. 11(3), 495-512. https://doi.org/10.1007/s13632-022-00851-0.
[4] Liu, H., Hu, D. & Fu, J. (2019). Analysis of MnS inclusions formation in resulphurised steel via modeling and experiments. *Materials*. 12(12), 2028, 1-16. https://doi.org/10.3390/ma12122028.
[5] Liu, J., Liu, C., Bai, R., Wang, W., Wang, Q., Zhang, H. & Ni, H. (2023). Precipitation and growth of MnS inclusions in non-quenched and tempered steel under the influence of solute micro-segregations during solidification. *Metallurgical and Materials Transactions B*. 54(2), 685-697. https://doi.org/10.1007/s11663-023-02718-3.
[6] Fu, P.X., Kang, X.H., Xia, L.J., Li, D.Z. & Li, Y.Y. (2010). Effect of microalloying on formation of inclusions in heavy Section high manganese steel casting. *China Foundry*. 59(12), 1337-1340.
[7] Su, L., Tian, J., Hu, S., Lv, M., Li, X., Qu, T., Wang, D. & Zhan, T. (2022). Effect of Ca/Mg on distribution and morphology of MnS inclusions in 45MnVS non-quenched and tempered steel. *Metals.* 13(1), 23, 1-16. https://doi.org/10.3390/met13010023.
[8] Shen, P. & Fu, J. (2019). Morphology study on inclusion modifications using Mg–Ca treatment in resulfurized special steel. *Materials*. 12(2), 197, 1-17. https://doi.org/10.3390/ma12020197.
[9] Liu, N., Tian, Q., Wang, Z., Xu, X. & Fu, J. (2023). Modification of MnS inclusion with trace tellurium to improve the machinability of medium-carbon low-sulfur

steel. *Ironmaking & Steelmaking*. 50(9), 1302-1310. https://doi.org/10.1080/03019233.2023.2197526.
[10] Shen, P., Yang, Q., Zhang, D., Yang, S. & Fu, J. (2018). The effect of tellurium on the formation of MnTe-MnS composite inclusions in non-quenched and tempered steel. *Metals*. 8(8), 639, 1-12. https://doi.org/10.3390/met8080639.
[11] Li, M.L., Wang, F.M., Meng, Q.Y., Tao, S.F. & Li, C.R. (2015). Effect of sulfur content on sulfide inclusions and microstructure in medium carbon non-quenched and tempered steel. *Journal of University of Science and Technology Beijing*. 37(2), 168-174. DOI:10.13374/j.issn2095-9389.2015.02.005.
[12] Li, M.L., Wang, F.M., Li, C.R., Tao, S.F. & Meng, Q.Y. (2016). In-situ observation of MnS effect on the tensile strength anisotropy of non-quenched and tempered steel. *Journal of University of Science and Technology Beijing*. 38(9), 1257-1263. DOI:10.13374/j.issn2095-9389.2016.09.009.
[13] Ma, M.T., Li, G.Z., Li, Z.G. & Lu, H.Z. (2008). The Effect of morphology and distribution of sulfides on mechanical properties and fatigue life of non-quenched and tempered steel. *Advanced Materials Research*. 51, 11-20. https://doi.org/10.4028/www.scientific.net/amr.51.11.
[14] Zhao, G.F., Wang, J.S., Wu, B. & Ma, C.Q. (2013). Quality control of non-quenched and tempered steel MnVS series produced by 50 t UHP EAF-LF-VD-CC flow sheet. *Special Steel*. 34(4), 43-45.
[15] Xiao, C., Zhang, J., Yuan, Y. & Luo, Y. (2012). Investigation on non-metallic inclusion of 49MnVS3 non-quenched and tempered steel. *Metalurgia International*. 17(1), 66.
[16] Liu, H., Hu, D., Wu, Y., Huang, Z., An, J. & Fu, J. (2018). Study of manganese sulfide precipitation in medium sulfur, non-quenched and tempered steel via experiments and thermodynamic calculation. *Metallurgical Research Technology*. 115(6), 605. https://doi.org/10.1051/metal/2018035.
[17] Shu, Q., Visuri, V.-V., Alatarvas, T. & Fabritius, T. (2020). Model for inclusion precipitation kinetics during solidification of steel applications in MnS and TiN inclusions. *Metallurgical and Materials Transactions B*. 51(6), 2905-2916. https://doi.org/10.1007/s11663-020-01955-0.
[18] Ren, W.-Q., Wang, L., Xue, Z.-L., Li, C.-Z., Zhu, H.-Y., Huang, A. & Li, C. (2021). A thermodynamic assessment of precipitation, growth, and control of MnS inclusion in U75V heavy rail steel. *High Temperature Materials and Processes*. 40(1), 178-192. https://doi.org/10.1515/htmp-2021-0022.
[19] Luo, Y., Zhang, J., Liu, Z., Xiao, C. & Wu, S. (2011). In situ observation and thermodynamic calculation of MnS in 49MnVS3 non-quenched and tempered steel. *Acta Metallurgica Sinica(English Letters)*. 24(4), 326-334.
[20] Yu, Q., Yang, X., Lai, C. & Tong, Z. (2021). Study on MnS inclusion aggregation along continuous casting slab thickness of medium carbon structural steel. *Metals*. 12(1), 56, 1-18. https://doi.org/10.3390/met12010056.
[21] Song, Y., Zhang, H. & Ren, L. (2024). A review of research on MnS inclusions in high-quality steel. *Engineering Reports*. 6(5), 1-21. https://doi.org/10.1002/eng2.12892.
[22] Liu, H., Huang, Z., Yu, D., Hu, D., Zhong, H., Zhai, Q. & Fu, J. (2019). Effect of cooling rate on microstructure and inclusion in non-quenched and tempered steel during horizontal directional solidification. *Journal of Iron and Steel Research International*. 26(9), 973-982. https://doi.org/10.1007/s42243-019-00282-2.
[23] Wu, M., Zhao, F., Yang, Y., Jiang, B., Zhang, C. & Liu, Y. (2017). The effect of size and distribution of MnS inclusions on the austenite grain growth in a low cost hot forged steel. *Steel Research International*. 89(2), 1-8. https://doi.org/10.1002/srin.201700270.
[24] Jiang, B., Wu, M., Sun, H., Wang, Z., Zhao, Z. & Liu, Y. (2018). Prediction model of austenite growth and the role of MnS inclusions in non-quenched and tempered steel. *Metals and Materials International*. 24(1), 15-22. https://doi.org/10.1007/s12540-017-7012-2.
[25] Xie, J., Hu, D., Fu, J. & Liu, H. (2018). Numerical analysis of effect of the solutes on formation of MnS in non-tempered steel. *Ironmaking & Steelmaking*. 46(6), 542-549. https://doi.org/10.1080/03019233.2018.1475453.
[26] Liu, N., Li, Y., Cheng, J. & Fu, J. (2024). Numerical understanding of MnS precipitation influence on solute micro-segregation during solidification. *Metallurgical Research Technology*. 121(5), 508. https://doi.org/10.1051/metal/2024061.
[27] Gui, L., Long, M., Huang, Y., Chen, D., Chen, H., Duan, H. & Yu, S. (2018). Effects of inclusion precipitation, partition coefficient, and phase transition on microsegregation for high-sulfur steel solidification. *Metallurgical and Materials Transactions B*. 49(6), 3280-3292. https://doi.org/10.1007/s11663-018-1401-x.